

Sequential replay of non-spatial task states in the human hippocampus

Nicolas W. Schuck^{1,2,*} & Yael Niv²

¹Max Planck Research Group NeuroCode

Max Planck Institute for Human Development, Lentzeallee 94, 14195 Berlin, Germany

²Princeton Neuroscience Institute and Department of Psychology
Princeton University, Washington Road, Princeton, NJ, 08544, USA

*Corresponding author contact:

Max Planck Research Group NeuroCode

Max Planck Institute for Human Development

Lentzeallee 94, 14195 Berlin, Germany

schuck@mpib-berlin.mpg.de

tel: +49 30 82406 649

Abstract

Neurophysiological research has found that previously experienced sequences of spatial events are reactivated in the hippocampus of rodents during wakeful rest. This phenomenon has become a cornerstone of modern theories of memory and decision making. Yet, whether hippocampal sequence reactivation at rest is of general importance also for humans and non-spatial tasks has remained unclear. Here, we investigated sequences of fMRI BOLD activation patterns in humans during wakeful rest following a sequential non-spatial decision-making task. We found that pattern reactivations within the human hippocampus reflected the order of previous task state sequences, and that the extent of this offline reactivation was related to the on-task representation of task states in the orbitofrontal cortex. Permutation analyses and fMRI signal simulations confirmed that these results reflected underlying BOLD activity, and showed that our novel statistical analyses are, in principle, sensitive to sequential neural events occurring as fast as one hundred milliseconds apart. Our results support the importance of sequential reactivation in the human hippocampus for decision making, and establish the feasibility of investigating such rapid signals with fMRI, despite its substantial temporal limitations.

Highlights

- We provide fMRI evidence for sequential pattern reactivation in the human hippocampus
- Sequences of patterns reflect states from a sequential, non-spatial decision-making task
- Simulations show that our novel fMRI analysis is sensitive to fast sequences of sub-second neural events
- Results support the importance of sequential reactivation in the human hippocampus for decision making

26 Introduction

27 The hippocampus plays an important role in memory¹⁻³, and is known to represent spatial
28 as well as non-spatial information that is relevant to an animal's current location within a
29 'map' of the ongoing task⁴⁻⁸. Recent research has suggested that hippocampal memories are
30 also used to inform spatial decision making and planing by reactivating neurally encoded
31 experiences that are relevant for the current task^{9,10}. Specifically, studies in rodents have
32 shown that hippocampal representations of spatial locations are reactivated sequentially
33 during short on-task pauses, longer rest periods, and sleep¹¹⁻¹³. This sequential reactivation,
34 or replay, is related to better planning¹² and memory consolidation¹⁴, and suppression of
35 replay-related short-wave ripples impairs spatial memory¹⁵.

36 While these findings have provided insights into the hippocampal computations under-
37 lying spatial decision making in animals, what role replay plays in non-spatial decision
38 making tasks in humans has remained unclear. We instructed participants to perform a
39 sequential non-spatial decision making task, and recorded functional magnetic resonance
40 imaging (fMRI) activity during resting periods before and after the task. The sequential
41 nature of the task was critical to correct performance, ensuring that participants would
42 encode sequential information while completing the task. We investigated whether sequences
43 of fMRI activation patterns during rest reflected hippocampal replay of task states. Evi-
44 dencing such replay, transitions between hippocampal fMRI activity patterns were related
45 to sequences of task states. Careful analyses and simulations confirmed that the structure
46 seen in hippocampal data reflects sequential information in the BOLD responses above and
47 beyond any structure introduced by state classifiers trained on task states. Importantly,
48 reactivation in the hippocampus during rest was associated with better representation of
49 the same task states in the orbitofrontal cortex during decision making, which in turn was
50 related to better performance of the task, in line with our previous work¹⁶.

51 Our results demonstrate sequential reactivation of non-spatial decision-making states
52 in the human hippocampus and suggest that the interaction between hippocampal and
53 prefrontal brain systems supports the construction and use of representations reflecting the
54 structure of the current task. Our findings, together with a set of rigorous statistical tests
55 and simulations, also establish the utility of noninvasive fMRI to detect possibly rapid replay
56 events, despite the low temporal resolution of this method.

57 Results

58 Thirty three human participants performed a sequential decision-making task that required
59 integration of information from past trials into a mental representation of the current task
60 state¹⁶ (see Methods). Specifically, each stimulus consisted of overlapping images of a face
61 and a house and participants' main task was to make age judgments (old or young) about
62 one of the images (Fig. 1A). The category to be judged (face or house) was instructed
63 before the first trial. Subsequent category switches were determined by the following rule:
64 if the age in the current trial was the same as the age in the previous trial, then the judged
65 category remained the same; on the other hand, if the age on the current trial was different
66 from the age on the previous trial, the participant had to switch to the other category from
67 the next trial onward (Fig. 1B). This created a 'miniblock' structure where each miniblock
68 involved judgment of one category. No age comparison was required on the first trial after
69 a switch. Miniblocks were therefore at least two trials long, and on average lasted for three
70 trials. These task rules resulted in a total of 16 'task states' reflecting the 'location' in
71 the current miniblock and were experienced in a structured order (Fig. 1C). For example,
72 the (Ho)Fy state, indicating a young face trial that followed an old house trial, was only
73 experienced at the end of a house (old) miniblock, as the first trial of the next face (young)
74 miniblock. This particular structure meant that although the task was not spatial, it involved
75 navigating through a sequence of states that had predictable relationship to each other, as
76 in a virtual maze. Participants performed the task with high accuracy (average error rate:
77 3.1%, time-outs: 0.6%, reaction time: 969 ms), improving their performance throughout the
78 course of the experiment (see Fig. 1D, significant linear trends of task block for reaction
79 times and errors, both p 's < .001, see also Supplemental Information, SI, Fig. S4, for further
80 details).

81 The experiment was comprised of two sessions during which participants engaged in the
82 above decision-making task while undergoing fMRI. The first session included ~ 5 minutes of
83 task instructions and four runs of task performance (388 trials, about 40 minutes duration).
84 The second session took place one to four days later and was identical to session 1, but
85 without instructions (Fig 1E). Resting state scans consisting of 5 minute periods of wakeful
86 rest without any explicit task or visual stimulation (100 volumes per resting state scan) were
87 administered for $N = 23$ participants (group 1) after session 1, before session 2 and after
88 session 2, resulting in a total of 300 whole brain volumes acquired during rest. A second
89 group of participants ($N = 10$; group 2) underwent the same procedures as group 1, plus
90 one additional resting state scan at the beginning of session 1, before having had any task

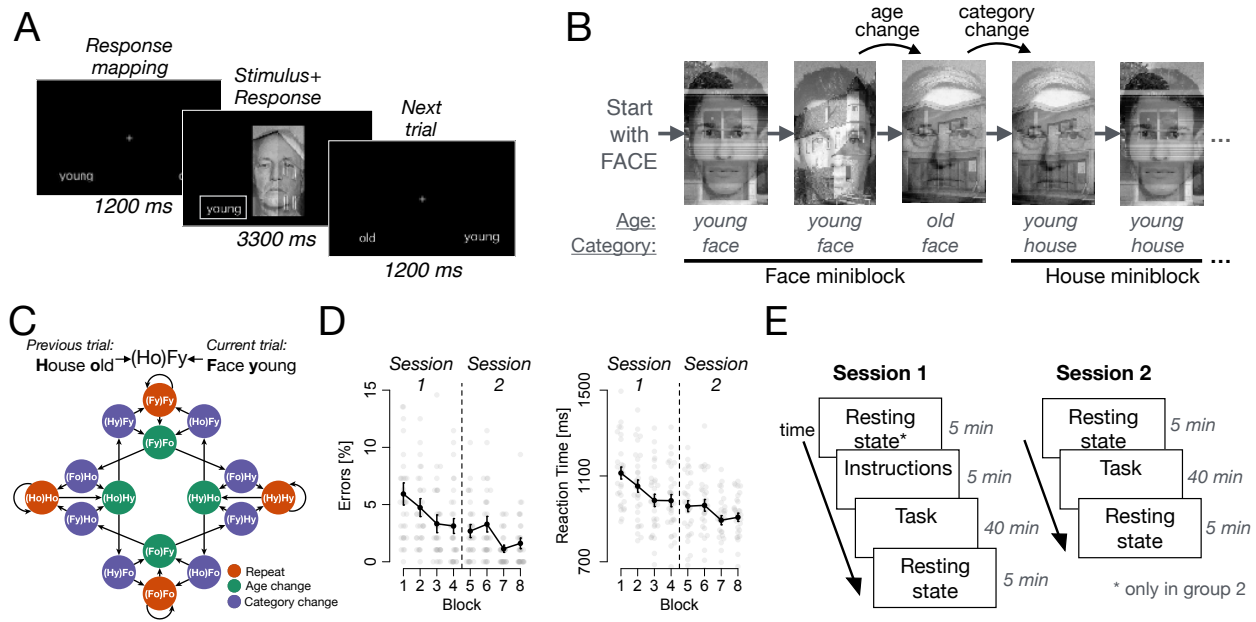


Figure 1: Experimental task and performance. (A): On each trial, participants had to judge the age of either a face or a house shown overlaid as a compound stimulus. Trials began with the display of a fixation cross and the response mapping (how left/right was assigned to old/young; 1200ms), followed by the stimulus. Responses could be made at any time, and the stimulus stayed on screen for an average of 3300 ms. (B): The task required participants to switch between judging faces and houses following each time the age changed between two trials, see text. (C): The state space of the task, reflecting the abstract space which participants traversed, analogous to a spatial maze although non-spatial from the point of view of the participant. Each node represents one possible task state, and each arrow a possible transition. All transitions out of a state are equally probable, occurring with $p = 0.5$. Each state of the task is determined by the age and category of the previous and current trial, indicated by the acronyms (see legend). States are colored based on their ‘location’ within a miniblock: trials within a miniblock in which the age and category were repeated (orange), trials at the end of a miniblock in which the age changed (green), and trials entering a new miniblock where the category changed (purple). (D): Average error rates and reaction times across the two sessions. Bars: ± 1 S.E.M. Grey dots represent individual subjects. (E): The experiment extended over two sessions, each of which included about 40 minutes task experience flanked by resting state scans. *: The pre-task resting state scan in Session 1 was performed only for a subgroup of our sample ($N = 10$; group 2).

91 experience (including being exposed to task instructions). This resulted in a total of 400
 92 whole brain volumes acquired during rest. The analyses reported below focus on fMRI data
 93 recorded during these resting scans. Resting-state data acquired after participants had task
 94 experience will from hereon be referred to as the TASK rest condition, whereas resting state
 95 data acquired before the task as the PRE rest condition. Data recorded while participants
 96 received instructions will serve as another control and be referred to as the INSTR condition.
 97 To account for differences in the number of data points constituting the TASK vs control
 98 conditions, we used a size-matched TASK condition where appropriate. Notably, while none
 99 of these conditions involves active experience of the sequential decision-making task, they
 100 differ in whether the task has been experienced before or not, and therefore in whether

101 hippocampal replay might be expected or not.

102 The main goal of our study was to investigate sequential reactivation, or replay, of
103 task-related experiences in the human hippocampus during rest. To this end, we trained
104 a multivariate pattern recognition algorithm (see Methods) to distinguish between the ac-
105 tivation patterns associated with each of the 16 task states in the data recorded during
106 task performance (Fig. 2A,B). Leave-one-run-out cross-validated classification accuracy
107 on the task data from the hippocampus (HPC) was significantly higher than chance and
108 than classification obtained in a permutation test (11.6% vs 7.1% in the permutation test,
109 $t_{32} = 8.9$, $p < .001$, chance level is 6.25%, Fig. 2C), indicating that hippocampal activation
110 patterns indeed reflected task states. We then applied the trained classifier to each volume of
111 fMRI data acquired during the resting state scans. Although classification accuracy cannot
112 be assessed for the resting scan data (due to lack of ground truth), we could assess the quality
113 of the classification using the mean unsigned distance to the decision hyperplane, a proxy
114 for classification certainty¹⁷. This distance was larger in the TASK condition compared to
115 simulated spatiotemporally-matched noise ('NOISE', $t_{32} = 12.9$, $p < .001$; for simulation
116 details see Methods and SI) and compared to the PRE condition ($t_9 = 2.1$, $p = .031$,
117 group 2 only, Fig. 2D). This suggests that fMRI patterns recorded during resting-state
118 scans following task experience could reflect reactivation of task states, in line with previous
119 findings^{18–20}.

120 The defining aspect of replay is that previously experienced states are reactivated *sequen-*
121 *tially*. We therefore asked next whether it is theoretically possible to measure rapid sequential
122 replay events (on the order of few hundreds of milliseconds in humans²¹) using fMRI, given
123 its low temporal resolution. To this end, we simulated fMRI activity that would result from
124 fast replay events (see SI and below), and asked what order and state information could be
125 extracted from these spatially and temporally overlapping patterns. The slow hemodynamic
126 response measured in fMRI causes brief neural events to impact the BOLD signal over several
127 seconds. Although these same dynamics might obscure the details of a replayed sequence,
128 our simulations showed that two successive fMRI measurements could still reflect two states
129 from the same sequence, for instance the first and last element of a multi-step replay event
130 (see SI). Because replay events mainly reflect short sequences of states¹³ (figure 3C in Ref.
131 13), if the activity we measured in the hippocampus at rest indeed reflects sequential replay,
132 we can therefore expect that consecutively decoded states be close in the task's state space
133 (that is, separated by few intervening states in Fig. 1C). This is analogous to the expectation
134 that spatial replay events would lead to sequential activation of place cells with place fields

135 nearby in space – even if some place cells were erroneously not identified as being active.
136 However, given the low accuracy of correctly decoding task states during task performance,
137 could we even expect to successfully decode a pair of states from the same replay event? Our
138 simulations showed that we could: because brain activity recorded after a rapid replay event
139 presumably includes several superimposed states (Fig. S5B), the likelihood of classifying
140 *one out of several* replayed states in each resting state brain volume is actually considerably
141 higher than the overall decoding accuracy when classifying a single prolonged event during
142 task. Our theoretical analysis showed that the chance that analyzing two consecutive brain
143 volumes results in decoding one (ordered) set of two states out of several possible sets caused
144 by the same replay event may be on the order of the overall decoding accuracy ($\sim 10\%$; see
145 SI).

146 Having established that, in principle, we can detect sequential replay in fMRI data, we
147 next investigated whether the sequences of states we decoded in the TASK resting data (Fig.
148 3A) reflected the sequential structure of the experienced task. We note up front that because
149 the classifier was trained on task data that were themselves sequential, signs of sequentiality
150 of classifier predictions might arise even in random noise—although clearly those data do not
151 reflect sequential replay. We therefore conducted a series of carefully controlled assessments
152 of the levels of sequentiality in our data to ensure that we were detecting true sequential
153 replay, and not merely unveiling the properties of the classifier. Indeed, we found in our data
154 several forms of sequentiality that are predicted by replay, above and beyond what we could
155 find in a series of closely matched controls.

156 First, we predicted that replay would be reflected in a smaller number of steps that
157 separate two consecutively decoded states, as indicated by the above-mentioned simulations.
158 In line with this idea, the number of steps between state transitions decoded in the TASK
159 resting condition was smaller, on average, than the distance between states in the INSTR
160 condition ($t_{32} = 2.4, p = .01$), smaller than the distance found in the PRE condition ($t_9 = 2.3,$
161 $p = 0.02$, group 2 only) and smaller compared to a permutation test in which classified states
162 were randomly reordered to control for overall state frequency (PERM condition: $t_{32} = 4.6,$
163 $p < .001$; Fig. 3B,C). Second, because replay events are separated by long pauses²¹, and
164 sequentiality should be present only following the replay events, we expected the occurrence
165 of short-distance state pairs to be clustered in time. Indeed, short-distance state pairs
166 (less than 3 steps apart) were not only more frequent than expected, but were also more
167 likely to occur in clusters in the TASK rest condition compared to the INSTR ($t_{32} = 1.7,$
168 $p = .046$), PRE ($t_9 = 1.9, p = .044$, group 2 only), and PERM controls ($t_{32} = 4.5, p < .001,$

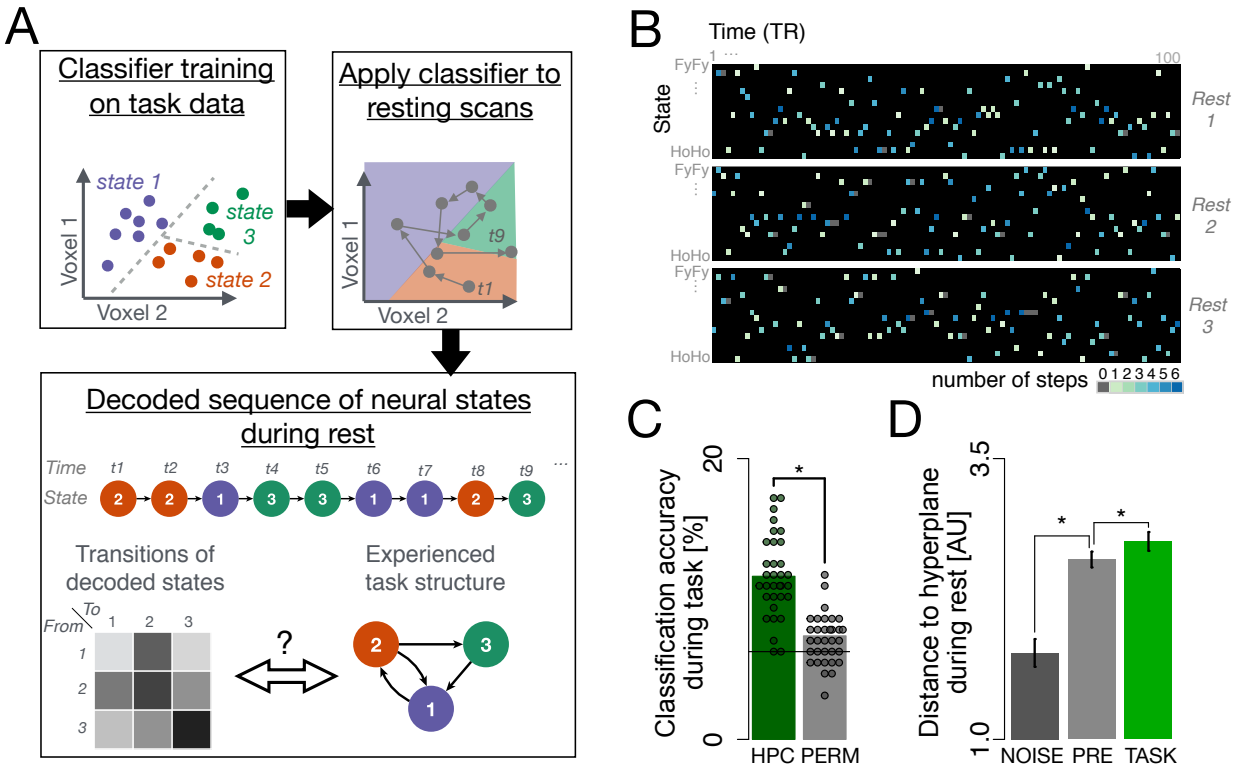


Figure 2: Sequential replay decoding analysis. (A): Illustration of analysis procedure. For simplicity, only two dimensions and three state classes are shown. We first trained a classifier to distinguish between the different task states in the hippocampal fMRI data acquired during the task. The trained classifier was then applied to each volume of fMRI data recorded during resting sessions (grey dots). This resulted in a sequence of predicted classifier labels that was then transformed into a ‘transition matrix’ T that summarized the frequency of decoding each pair of task states consecutively. The structure of the decoded sequences, as summarized by this matrix, was then compared to the sequential structure of the task (see text). Note that the real analysis involved 16-way classification of >1000 dimensional data, which was compared to the task state space shown in Fig. 1C. (B): Example data from one randomly selected participant. Each dark rectangle illustrates the sequence of classified states for the 100 volumes of fMRI data recorded in one resting state scan (depicted are three resting state scans acquired throughout the experiment; see Fig. 1E). Columns represent time, and rows states. Each color-filled cell represents the state classified at the respective time point, and color indicates the distance (in steps in the state space; Fig. 1C) from the state decoded in the previous timepoint (i.e., the previous TR). (C) Classification accuracy during task performance was significantly higher in hippocampal data (HPC) than in a permutation test (PERM). The solid line represents the theoretical chance baseline of $100/16=6.25$. (D): Average distance to the hyperplane for classified states during rest in the NOISE (dark grey, left bar), PRE (light grey, middle bar, $N=10$) and TASK conditions (green, rightmost bar, $N=33$). Larger distance indicates higher certainty in the classification of the state. Each dot indicates one participant, bars within-subject S.E.M., *: $p < .05$.

169 Fig. 3D). Next, we ensured that the above results could not be explained by sustained
 170 state activation, or only one particular decoded state distance. To this end, we removed
 171 state repetitions (“self transitions”) from the data and tested whether the prevalence of
 172 each step size (a transition between two states separated by k steps) was linearly related
 173 to the distance between the two states in task space. In other words, we tested whether

174 the empirical frequency of decoding each pair of task states consecutively (the “transition
175 probability” for each pair of decoded states, summarized in matrix T ; Fig. 3A) was negatively
176 correlated with the distance D between the states in the task (where D_{ij} corresponds to
177 the minimum number of steps necessary to get from state i to state j ; Fig. 3E). The
178 correlation between T and D was indeed significantly negative (average $r = -.16$, $t_{32} =$
179 -17.7 , $p < .001$, t-test of individual correlations across participants, Fig. 3F), and was
180 substantially more negative than the correlation seen in the PERM control ($r = -.08$,
181 $p < .001$, reflecting an effect of overall state frequency; $\Delta r = -.07$, $t_{32} = -5.8$, $p < .001$).
182 Applying the trained classifier to matched fMRI noise (NOISE control, see Methods and SI,
183 Fig S1) also resulted in a negative correlation ($r = -.08$, $p < .001$, showing that temporal
184 contingencies between states in the classifier training data can lead to spurious correlations),
185 which was nevertheless significantly weaker than the correlation found in the TASK rest data
186 ($\Delta r = -.08$, $t_{32} = -5.6$, $p < .001$, Fig. 3G). Importantly, our hypothesis that sequential
187 reactivation of task-state representations during rest was caused by task experience was
188 also supported by a significantly stronger anti-correlation between T and D in the TASK
189 condition as compared to the INSTR data ($t_{32} = -12.1$, $p < .001$, when comparing a subset
190 of the TASK condition matched in number of TRs to the INSTR data), as well as the PRE
191 resting scan ($t_9 = -7.9$, $p < .001$, group 2; $p = .059$ when compared to only the first resting
192 scan in TASK condition), as shown in Fig. 3H. Finally, we also assessed the effect of the
193 sequential structure in the training data on our results in an additional control analysis in
194 which we systematically excluded sets of state pairs from classifier training (see SI, Fig.
195 S2), to test if, as a result, these pairs would seem to have a lower transition frequency in
196 the resting data. This concern was allayed as the excluded transitions were observed as
197 often as the included transitions ($t_{32} = 0.3$, $p = 0.73$), in line with our conclusion that
198 the transition frequencies observed during rest reflected sequential reactivation above and
199 beyond any sequential structure in the classifier.

200 In order to investigate the effects of task experience on pair-decoding frequency data T
201 while simultaneously (a) excluding state repetitions, (b) controlling for the above-mentioned
202 effect of temporal contingencies in the classifier training and (c) incorporating the different
203 sources of between- and within-participant variability, we performed a logistic mixed-effects
204 analysis. In this, we modeled both the effect of interest (D) and nuisance covariates that
205 could potentially affect T (see Methods). We will henceforth call the effect estimate (beta
206 weight) of the distances D on the data T in this model ‘sequenceness,’ and the nuisance
207 effects ‘randomness.’ Comparing a model of the frequency of transitions T that contained

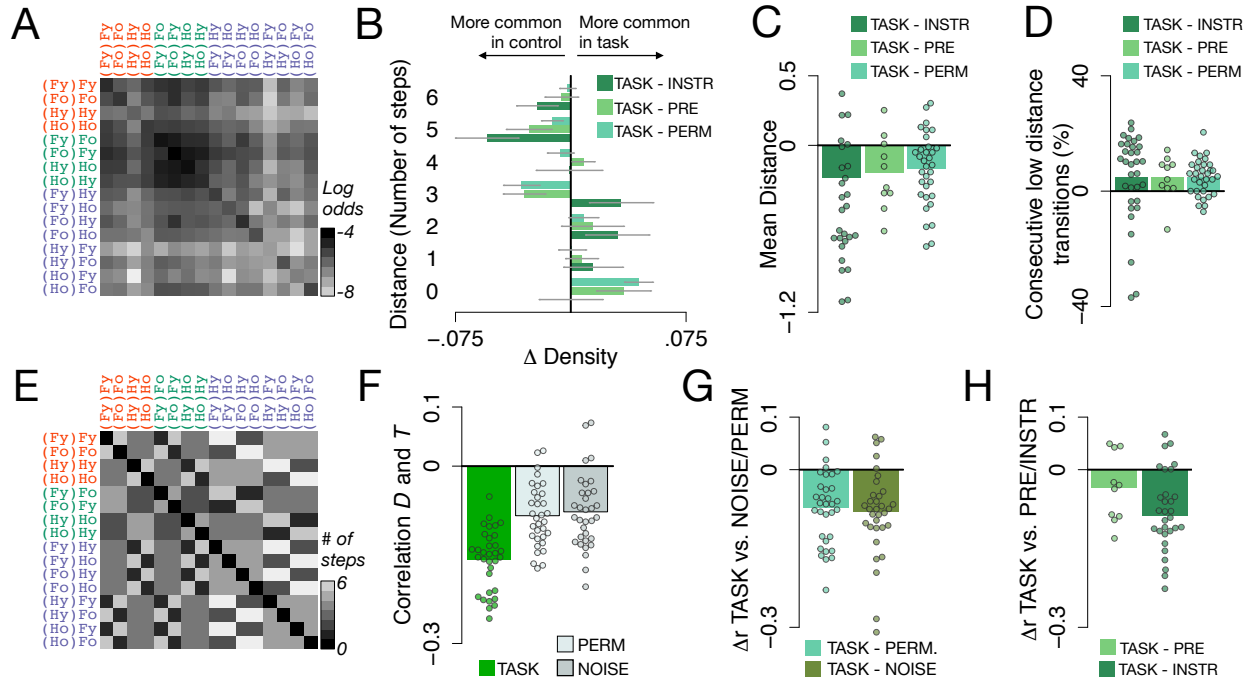


Figure 3: Hippocampal state transitions during rest are related to state distances in the task. (A): The matrix T , expressing the log odds of transitions between all states in the sequence of classification labels in the hippocampal TASK rest data, averaged across all participants. Y-axis: first state, x-axis: second state, in each consecutively decoded pair. Darker colors reflect a higher probability of observing a pair in the data. (B): Relative distributions of number of steps separating two consecutively decoded states. A distance of 1 corresponds to a decoded state transition as experienced in the task, 2 corresponds to a transition with one item missing in between as compared to the task, etc. Barplots show the difference in relative frequency (Δ Density) with which each transition type was observed in the TASK condition compared to INSTR and PRE control conditions and a permutation test (PERM), see legend. Smaller distances are more frequently observed in the TASK data, whereas larger distances are more common in the control data, suggesting that the TASK resting-state data reflect reactivation of short sequences (C): The average distance in state space of two consecutively decoded states was significantly lower in the TASK data as compared to the INSTR, PRE and PERM controls (all $ps < .05$, t-test comparing difference to 0). (D): Low-distance transitions (fewer than 3 steps) occurred in succession significantly more frequently in the TASK data compared to all controls (all $ps < .05$). (E): The matrix D , indicating the minimum number of steps between each pair of states in the task (i.e. the state distances). Lighter colors reflect larger distance between states. (F): Average correlations between the state distance matrix D and the corresponding decoded transition matrix T in the TASK condition (green bar, left), as compared to a permutation test (PERM; light grey, middle) or when the same classifier was applied to participant-specific spatio-temporally matched noise (NOISE; dark gray bar, right, see also Fig. S1). (G): Within-participant differences between correlations in TASK versus the PERM and NOISE controls (all $ps < .05$) (H): The anti-correlation between D and T in the PRE and INSTR phases was lower than in the TASK resting state sessions (matched in amount of data compared). Dots reflect differences in correlations for individual participants.

208 only randomness regressors with a model that also included the sequenceness (task distances)
 209 regressor D , we found no difference in model fit in the PRE rest condition (Aikake Infor-
 210 mation Criterion, AIC, 3651.4 vs. 3651.5 for the model without and with the sequenceness
 211 regressor, respectively, $\chi^2_1 = 1.9$, $p = .17$). In the TASK rest condition, in contrast, adding
 212 the sequenceness regressor improved model fit significantly (AIC 3645.4 vs. 3642.1, lower

213 numbers indicate a better fit, $\chi_1^2 = 5.2$, $p = .02$, group 2 only and considering only the first
214 TASK resting scan from the first session to equate power with the PRE analysis above).
215 Indeed, the difference between the two datasets was statistically significant: including both
216 PRE and TASK conditions within one model showed improved fit when the interaction of
217 condition factor with sequenceness and randomness was included (AIC 3660.2 vs. 3674.1,
218 $p < .001$). Figure 4A,B shows the sequenceness and randomness effects in the TASK
219 compared to the PRE condition. Comparing the INSTR to the TASK condition in all
220 participants showed the same pattern of effects: No effect of the sequenceness regressor was
221 found in the INSTR condition (AIC 10046 vs 10047, $p = .27$), but there was a significant
222 effect in the TASK rest condition (AIC 10130 vs. 10146, $p < .001$, TASK data matched
223 in size to equate power), see Figure 4C,D. However, here the combined model indicated no
224 interaction between condition and sequenceness vs. randomness (10142 vs 10130, $p > .1$).
225 Note that the lack of sequenceness before task experience shows that our modelling analysis
226 successfully controlled for bias effects due to the temporal contingencies between states in the
227 classifier training data. Analyzing data from all participants (groups 1 & 2) and all TASK
228 resting-state scans with this model indeed showed that the inclusion of a state distance
229 factor led to significantly better model fits even after controlling for the randomness (bias)
230 effect as above (AIC 10789 vs 10780, $\chi_1^2 = 11.0$, $p < .001$), supporting the conclusion that
231 previously experienced sequences of task states are replayed in the human hippocampus
232 during rest periods. These results were unaffected by the choice of distance metric, see SI.
233 No comparable pattern of results emerged when data from the orbitofrontal cortex, a brain
234 area known to contain task-state information during decision making^{16,22}, were analyzed in
235 a similar fashion (see SI).

236 The above analyses relied on the forward distance between states, as experienced during
237 the task. We next tested whether the sequenceness found in the TASK condition could be
238 explained better by alternative forms of replay, namely backward replay or forward replay of
239 partial states such as the stimuli experienced. To this end, we defined alternative distance
240 matrices corresponding to the above hypotheses, and tested the power of these alternative
241 models to explain the sequences of states decoded during rest. For these analyses, instead
242 of distances we used one-step task transition matrices to avoid statistical disadvantages of
243 alternative models that have very evenly distributed distances (high entropy). As in our
244 original analysis, all 1-step matrices were based on the task state diagram. The alternative
245 1-step matrices were created by either transposing the original 1-step matrix (backward
246 analysis) or by assuming that only partial aspects of each trial's state are represented,

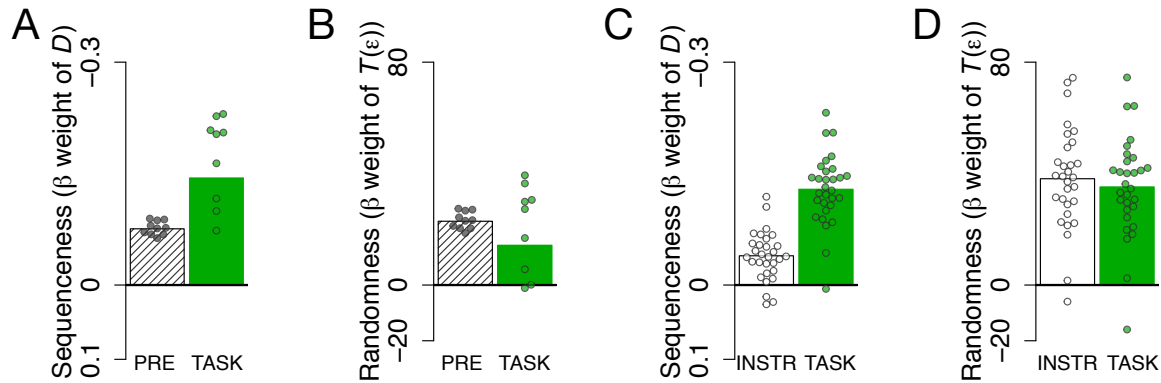


Figure 4: Effect of state distance (sequenceness) on transition frequency in hippocampal data is specific to TASK rest conditions. Bars indicate strength of fixed effects in mixed effects model (see text). Dots indicate individual random effects. Note that variability of dots in this case cannot be used to infer significant differences. (A): Effect of sequenceness regressor D on resting data from the PRE and TASK conditions. Model comparisons based on AIC showed that the sequenceness regressor led to better model fit in the TASK but not the PRE condition. (B): Effect of randomness across the PRE and TASK conditions. The randomness regressor $T(\epsilon)$ captures the sequentiality in the data due to classifier bias, see Methods. (C): Sequenceness in the INSTR and TASK conditions, as in panel (A). Adding the sequenceness regressor led to better model fit only in the TASK condition. (D): Randomness in the INSTR and TASK conditions as in panel (B).

247 for instance by computing the experienced transitions between attended stimuli without
248 representing the events in the previous trial (see Methods). As the classifier was trained
249 to distinguish all 16 possible states, we assumed that different states corresponding for
250 instance to the same stimulus would be fully aliased. We tested four alternative hypotheses
251 by calculating the likelihood that the observed sequences of states were generated by (a)
252 replay of states containing the stimulus on the current trial ('stimulus model', Fig. 5A), (b)
253 replay of states containing only information about the currently attended category ('category
254 model', Fig. 5B), (c) replay of states containing information about the attended category on
255 the current and previous trial ('category memory model', Fig. 5C), and (d) backward replay
256 of full states, in the opposite order as they were experienced ('backward model', Fig. 5D),
257 and comparing these to the likelihood of the data being generated by forward transitions
258 between full states (the one-step version of our original hypothesis; 'full state model', Fig.
259 5E). Model comparison using the same mixed effects models as above showed that the 1-step
260 transitions assuming full state representation (Fig. 5E) led to a better model fit compared
261 to all four alternative models (AIC: 20808, 20808, 20806, 20796, for the 4 alternative models,
262 respectively; AIC of true model: 20782, see Fig. 5F).

263 Similar to our above analyses investigating the theoretical possibility of decoding fast
264 replay states from fMRI data, we also test whether the observed sequenceness in hippocampal
265 fMRI data could have been caused by fast sequences of neural events in principle. For this

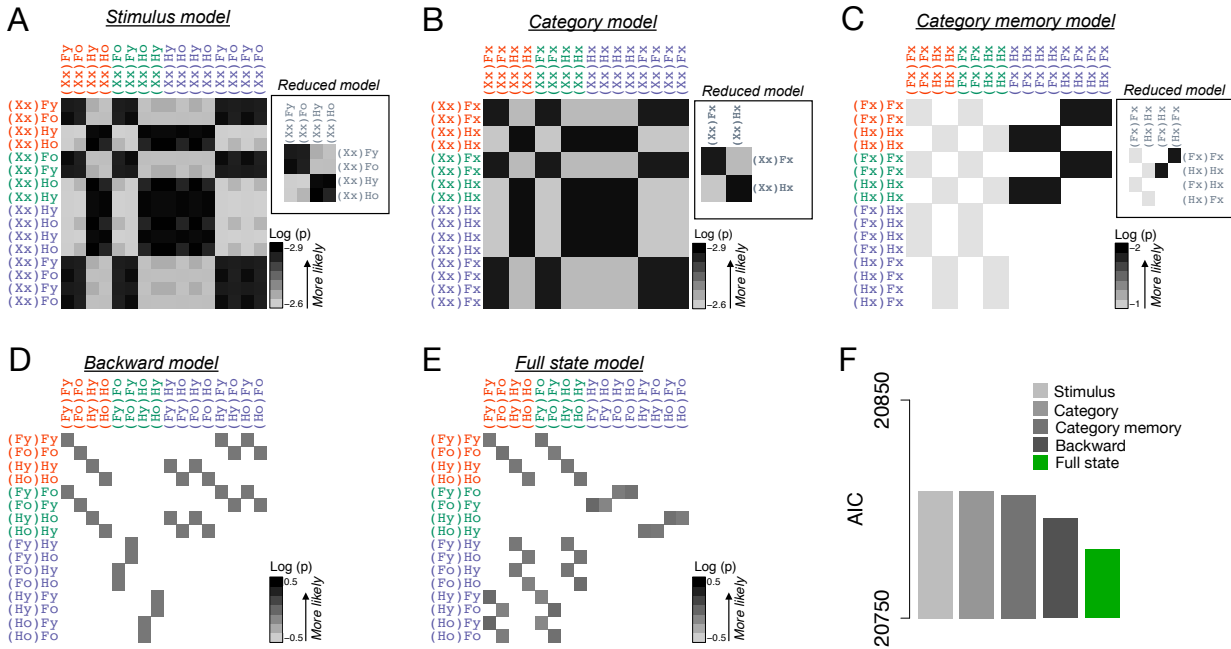


Figure 5: Alternative state transition matrices do not explain hippocampal state sequences during rest. (A-E) Alternative state transition matrices. Rows indicate origin states and columns indicate receiving states for a given transition, see text. Color shading indicates log likelihood of the corresponding 1-step transition under each alternative hypothesis, see legend and Methods. Empty (white) cells indicate that a transition is not possible. 'Reduced model' panels in A-C show the transition matrix when aliased states are collapsed. (E) Corresponds to the one-step transitions for our original hypothesis (compare to Fig. 3E). (F) Akaike information criterion (AIC) when data from the TASK rest condition were modelled using the transition matrices shown in A-E. The full state model explained the data best (lower AIC scores indicate a better model fit).

266 we simulated fMRI signals generated by sequences of hypothetical neural events occurring
 267 at different speeds, and asked at which speed the above analyses can uncover the underlying
 268 sequential structure. In these simulations, each neural event triggered a hemodynamic
 269 response in a distributed pattern of voxels (see SI; Fig. S3). When the signal-to-noise ratio
 270 was adjusted to yield state-decoding levels that were matched to our data (12.1% accuracy
 271 in simulations, vs. 11.6% in the data), significant correlations between the consecutively
 272 decoded state pair frequencies T and the corresponding distances D were found even at
 273 replay speeds of about 14 items per second (i.e. inter-event intervals of 60-80ms, $r = -0.018$,
 274 permutation test: $r = -0.003$, t-test of sequence vs permutation results $t_{199} = -4.42$,
 275 $p < .001$, corrected for multiple comparisons; corresponding test for events separated by
 276 faster events at 40-60 ms: $p = .18$; $p < .05$ for all slower sequences; Fig. S5 and S6). This
 277 supports our conclusion that our findings in the resting-state data may reflect fast sequential
 278 replay in the human hippocampus.

279 In combination, these analyses show that sequences of hippocampal fMRI activity pat-
280 terns during rest were systematically related to previous task experience. Interestingly, we
281 found no such effect when we included backward distances between states instead of the
282 forward distance in the model. This indicates that the sequences of hippocampal activity
283 patterns became directionally structured in correspondence to participants' task experience,
284 and suggests that the hippocampus was engaged in forward replay in the post-task rest
285 period.

286 Finally, we investigated the functional significance of hippocampal replay of abstract
287 task states. One idea is that replay helps to form, or further solidify, a representation of the
288 transitions between states of the task²³⁻²⁵. We therefore tested for a relationship between
289 sequential state reactivation during rest and better representation of states during the task,
290 as measured through cross-validated state decoding accuracy in fMRI data recorded during
291 task performance. We did not find any evidence of a relationship between hippocampal
292 sequenceness at rest and decoding of states during task performance ($r = -.05$, $p > .05$).
293 However, we did find a significant correlation between hippocampal sequenceness at rest
294 and state representations in the orbitofrontal cortex during the task ($r = -.47$, $p = .005$).
295 Notably, in previous work we have shown that improved state decoding in the orbitofrontal
296 cortex is associated with better decision making in this task, see¹⁶. Indeed, in the current
297 dataset we also found a relationship between the change in orbitofrontal decoding accuracy
298 during the task and improvements in task performance. That is, runwise decoding within
299 the first session was correlated with runwise error rates ($\chi^2_1 = 9.1$, $p = .003$, using the
300 same decoding measure as used before, see ref. 16). This was not the case for on-task
301 decoding in the hippocampus ($p = .87$, interaction with ROI: $\chi^2_1 = 5.2$, $p = .023$). This
302 finding therefore suggests a role for hippocampal replay in supporting the integrity of task-
303 relevant orbitofrontal state representations during decision making. We also tested for a
304 direct relationship between hippocampal replay at rest and behavioral measures of task
305 performance, but did not find any evidence for a relationship between sequenceness and
306 reaction times, error rates, or the change in these measures across runs (all $ps > .10$).
307 Together, these results suggests that hippocampal replay supports the offline formation or
308 maintenance of a 'cognitive map' of the task, while the orbitofrontal cortex is deployed to
309 represent such a map during decision making^{16,26}.

310 Discussion

311 Our findings demonstrate that fMRI patterns recorded from the human hippocampus dur-
312 ing rest reflect sequential replay of non-spatial task states previously experienced in a
313 decision-making task. Previous studies have relied on sustained elevated fMRI activity in
314 the hippocampus or sensory cortex as evidence for replay^{18–20,27}, investigated wholebrain
315 MEG signals²⁸, or studied EEG sleep spindles and memory improvements that are thought
316 to index replay activity^{29–33}, but were not able to directly demonstrate sequential replay in
317 the human hippocampus. Our study represents an important extension of these findings by
318 providing evidence of sequential offline reactivation of non-spatial decision-making states in
319 the human hippocampus.

320 Evidence of sequentiality and localization of replay in the human hippocampus is in
321 direct correspondence with animal studies in which replay has been shown to be sequential
322 and specific to hippocampal place cells, e.g.³⁴. Importantly, unlike the majority of previous
323 investigations in animals, the here reported sequences of activation patterns signify the
324 replay of non-spatial, abstract task states. Our results therefore add to a growing literature
325 proposing a significant role for ‘cognitive maps’ in the hippocampus in non-spatial decision
326 making^{3,8,26,35}.

327 Our findings are in line with the idea that the human hippocampus samples previous
328 task experiences in order to improve the current decision-making policy, a mechanism that
329 has been shown to have unique computational benefits for achieving fast and yet flexible
330 decision making^{23–25}. Dating back to Tolman³⁶, this idea requires a neural mechanism that
331 elaborates on and updates abstract state representations of the current task, regardless of the
332 task modality. Several studies have suggested that the hippocampus and adjacent structures
333 support a broad range of relational cognitive maps³⁵, as evidenced by hippocampal encoding
334 of not only spatial relations but also temporal^{37,38}, social⁷, conceptual⁶ or general contingency
335 relations³⁹. Here, we showed that the human hippocampus not only represents these abstract
336 task states, but also performs sequential offline replay of these states during rest.

337 Our results imply a relationship between hippocampal replay and the representation of
338 decision-relevant task states that are thought to reside in the orbitofrontal cortex^{16,22,40–42}.
339 The relationship between ‘offline’ hippocampal sequenceness and the fidelity of ‘online’
340 orbitofrontal task-state representations raises the possibility that the hippocampus supports
341 the maintenance and consolidation of state transitions that characterize the task and are
342 employed during decision making³⁸. Given our findings—and recent evidence implicating
343 hippocampal place and entorhinal grid cells in signaling non-spatial task-relevant stimulus

344 properties^{6,8}—a crucial question for future studies will be to further specify how flexible, task
345 specific representations in the hippocampus interact with task representations in other brain
346 regions²⁶. Of particular interest will be investigations asking whether neural populations in
347 the hippocampus and entorhinal cortex share a common neural code for abstract task states
348 with orbitofrontal¹⁶ and medial prefrontal regions⁴³, as indicated by recent studies^{6,44,45}.
349 Together with our findings, this research promises to shed light on the neural representations
350 and computations underlying memory and decision making.

351 **Experimental Procedures**

352 **Participants**

353 Thirty nine participants were selected according to standard fMRI screening criteria (right
354 handedness, 18–35 years of age, normal or corrected-to-normal vision and no contraindication
355 for fMRI) from the Princeton University community, and were compensated with \$20 per
356 hour plus up to \$5 performance-related bonus. Six participants were excluded from analysis
357 due to either technical errors (3 participants), violation of performance criteria standards (2
358 subjects with over 3 times the average error rate in the last two blocks of the experiment)
359 or incomplete data (1 participant). The final sample consisted of 33 participants (22 female,
360 mean age 23.4 years). All participants provided informed consent and the study was approved
361 by Princeton University’s Institutional Review Board.

362 **Stimuli**

363 Stimuli consisted of spatially superimposed images of a face and a house (see¹⁶; face images
364 from <http://faces.mpg.de/faces> described in⁴⁶, see Fig. 1). Faces and houses could
365 be classified as either young or old, e.g. a stimulus could show an old face image blended
366 with a contemporary (i.e., young) house image. Four classes of stimuli were possible: (1)
367 two old or (2) two young face and house pictures, (3) a young face with an old house or (4)
368 vice versa.

369 **Task**

370 The task was identical to Schuck et al. 2016 and will be described only briefly. Each trial
371 began with the display of the mapping of a left and right key to a young and old response
372 (changing randomly trialwise) below a fixation cross for 1.2s (range: 0.5–3.5s). Then, a

373 compound face-house stimulus was shown for 3.3s (range: 2.75-5s; Fig. 1) and participants
374 had to make an age judgment about one of the two image categories. Participants knew
375 which category of the stimulus they had to judge by applying the following rules: 1. before
376 the first trial of each run, the category to judge was displayed on the screen; 2. Once the age
377 of the relevant category changed (e.g., from young to old), the judged category changed on
378 the next trial. 3. No age comparison was necessary on the first trial after a category change,
379 i.e. each category was judged for at least two trials in a row before a switch. The average
380 trial duration was 4.5s (range: 3.25-8.5s), all timings were randomly drawn from a truncated
381 exponential distribution and the response deadline was 2.75s. The category instruction cue
382 at the beginning of a run was displayed for 4s. Erroneous or time-out responses led to
383 feedback (written above stimulus for 0.7s) and trial repetition. If an error trial involved an
384 age change (and thus would require a category switch on the next trial), participants had to
385 repeat the trial before the error as well as the error trial, giving them the chance to observe
386 the age change. Otherwise, they had to repeat the trial on which they made the error.

387 **Design**

388 Participants underwent two fMRI sessions. The first session began with the display of
389 written instructions while participants underwent a functional scan (group 1), or a 5 minute
390 resting-state scan followed by instructions (group 2). The instructions explained the rules of
391 the task and contained a training phase in which simple age judgments had to be made on
392 (non-overlapping) face and house images. The images shown in this period were later used in
393 the task, thus familiarizing participants with the age judgment aspect of the task as well as
394 the stimuli. The instructions furthermore involved an annotated walk-through of four trials
395 of the real task (i.e., with overlapping images and the requirement to switch attention after
396 an age change). Following the instructions, participants performed 4 runs of the task (97
397 trials per run, 388 total). Each run lasted about 7-10 minutes and participants were given
398 the chance to rest briefly between runs. A 5 minute fieldmap scan was done between runs
399 2 and 3, resulting in a longer break for participants. After run 4, participants underwent a
400 resting state scan as well as a structural scan. Lights were turned off during resting-state
401 scans and participants were instructed to stay awake for the entire duration of the scan (5
402 minutes, 100 TRs). The second session was identical for all participants and involved the
403 following scans: resting state, 2 task runs, fieldmap, 2 task runs, resting state and structural
404 scan. Thus, overall, participants performed 8 task runs and 3 (group 1) or 4 (group 2)
405 resting-state scans. In all other regards, the task design involved the same characteristics as

406 detailed in Schuck et al. (2016).

407 Behavioral Analyses

408 Behavioral analyses were done using mixed effects models implemented in the package lme4⁴⁷
409 in R⁴⁸. The model included fixed effects for Block, Condition, Category and intercept.
410 Participants were considered a random effect on the intercept and the slopes of all fixed
411 effects. The reported p -values correspond to Wald chi-square (χ^2) tests as implemented in
412 R. Reaction time (RT) analyses were done on error-free trials only and reflect the median
413 RT within each factor cell.

414 fMRI Scanning Protocol

415 Magnetic-resonance images were acquired using a 3-Tesla Siemens Prisma MRI scanner
416 (Siemens, Erlangen, Germany) located at the at the Princeton Neuroscience Institute. A
417 T2*- weighted echo-planar imaging (EPI) pulse sequence was used for functional imaging
418 (2×2 mm in plane resolution, TR = 3000 ms, TE = 27 ms, slice thickness = 2 mm, 53 slices,
419 96×96 matrix (FOV = 192 mm), iPAT factor: 3, flip angle = 80° , A→P phase encoding
420 direction). Slice orientation was tilted 30° backwards relative to the anterior – posterior
421 commissure axis to improve acquisition of data from the orbitofrontal cortex⁴⁹. Field maps
422 for distortion correction were acquired using the same resolution (TE1 = 3.99ms) and a
423 MPRAGE pulse sequence was used to acquire T1-weighted images (voxel size = 0.9^3 mm).
424 The experiment began 20 seconds after acquisition of the first volume of each run to avoid
425 partial saturation effects.

426 fMRI Data Preprocessing

427 FMRI data preprocessing was done using SPM8 (<http://www.fil.ion.ucl.ac.uk/spm>)
428 and involved fieldmap correction, realignment, and co-registration to the segmented struc-
429 tural images. The task data used to train the classifier were further submitted to a mass-
430 univariate general linear model that involved run-wise regressors for each state (see below),
431 nuisance regressors that reflected participant movement (6 regressors) and run-wise inter-
432 cepts. The resulting voxelwise parameter estimates were z-scored and spatially smoothed (4
433 mm FWHM). The resulting activation maps were used as the training set for a support-vector
434 machine with a radial basis function (RBF) kernel that was trained to predict the task state
435 from which a particular activation pattern came from LIBSVM⁵⁰. Like the activation maps

436 used for classifier training, the resting-state data were z-scored and smoothed (4mm FWHM).
437 Anatomical ROIs were created using SPM's `wfupick` toolbox. The hippocampus (HC) was
438 defined as the left and right hippocampus AAL labels. The orbitofrontal cortex was defined
439 as in¹⁶. Behavioral analyses and computations within the assumed graphical model of state
440 space (see below) were done using R⁴⁸.

441 **fMRI Classification Analysis**

442 The support vector machines were trained on 8 maps of parameter estimates (“betas”) for
443 each of the 16 states (one map for each state and run) restricted to the anatomical mask
444 of the hippocampus (back-transformed into each subject’s individual brain space) or the
445 orbitofrontal cortex. Classification accuracy was assessed with a leave-one-run-out cross-
446 validation scheme in which data from 7 runs were used for training and the held-out run was
447 used for testing (Fig. 2). The resting-state analysis used a classifier trained on all available
448 task data (8 runs). This classifier was applied to each volume of the resting-state data
449 and the most highly classified state was considered as the output of the classifier for that
450 volume. The resulting sequence of predictions was the main focus of our analyses (see below).
451 We obtained the distance to the hyperplane by dividing the decision value by the norm of
452 the weight vector w , as specified in the libSVM webpage (<http://www.csie.ntu.edu.tw/~cjlin/libsvm/faq.html#f4151>). For each volume, we then calculated the average of the
454 distances of all pairwise comparisons of the predicted class against all other classes, to obtain
455 a proxy of how certain the classifier is in its prediction. Student t tests pertaining to decoding
456 results were one-tailed, given the *a priori* expectation of larger-than-chance decoding in the
457 hippocampus.

458 **Sequenceness Analysis**

459 The main question of the sequenceness analysis was whether the state transitions decoded
460 from resting state scans, T , were related to the distance between states experienced during
461 the task, D . To this end, we analyzed the neural state transitions T with logistic mixed-effects
462 models, using the `lme4`⁴⁷ package in R⁴⁸. Because the slow hemodynamic response function
463 leads to encoding of sequential structure in activity patterns (i.e., there is high similarity
464 between temporally adjacent patterns), a classifier trained on sequential task data can be
465 biased to decode states in a similar sequence to the training data, even if the test data are
466 random (i.e., the ‘sequenceness’ identified in the test data comes from the training data,

467 not the test data). We therefore applied the trained classifier to matched fMRI noise (see
468 below) and used the resulting spurious ‘state transitions,’ $T(\epsilon)$, as a covariate that would
469 account of the spurious base rate of transitions that is due to the classifier rather than the
470 data. Applying these models to control conditions consistently yielded non-significant effects
471 of sequenceness, showing that this analysis appropriately controls for the above mentioned
472 spurious structure that is observable for instance in the significant correlations between D
473 and T in the noise data (Fig. 3F). Specifically, our model included the following fixed effects:
474 (1) the distance between states, D , which was the regressor of interest, and as regressors of
475 no interest (2) the transition probabilities obtained in the above mentioned noise simulations,
476 $T(\epsilon)$, (3) an orthogonal quadratic polynomial of $T(\epsilon)$ that was included in order to account
477 for as much noise-related variance as possible, and (4) an intercept. Models of change
478 in sequenceness across PRE, INSTR and TASK conditions (Fig. 4) additionally involved
479 interaction terms of condition with the distance D and condition with the noise transitions
480 $T(\epsilon)$. Participant identity was included as a random factor to account for between subject
481 variability. To capture state-related variability (state frequency effects affect the distribution
482 of state transitions), state identity s_j of a transition from state i to state j was used as an
483 additional random effect nested within subject. Participant and state were random grouping
484 factors for all fixed effects with exception of the quadratic expansion of $T(\epsilon)$, where including
485 these random factors caused problems in fitting the logistic regression models.

Formally, the model followed the general assumption that the number of transitions Y is drawn from a binomial distribution of n draws and probability T :

$$Y_{ijk} \sim B(n_k, T_{ijk})$$

486 where n_k corresponds to the number of measurements for subject k , and i and j index
487 the outgoing and incoming states of a given transition. The logit transformed probabilities
488 T (shown in Fig. 2D; logit is the canonical link function for binomial models) were then
489 modeled in a mixed effects regression model with the above mentioned fixed and random
490 effects structure:

$$\begin{aligned} \text{logit}(T_{ijk}) = & \beta_0 + D_{ij}\beta_1 + T(\epsilon)_{ij}\beta_2 + T(\epsilon)_{ij}^2\beta_3 + \\ & \gamma_{0k} + D_{ij}\gamma_{1k} + T(\epsilon)_{ij}\gamma_{2k} + \\ & \zeta_{0kj} + D_{ij}\zeta_{1kj} + T(\epsilon)_{ij}\zeta_{2kj} + \epsilon_{ijk} \end{aligned}$$

491 In the text, we describe the fixed effect of D , β_1 in the models, as ‘sequenceness,’ and the
492 fixed effect of $T(\epsilon)$, β_2 , as ‘randomness’ (Fig. 4B,C). The subject-specific random effects of

493 D , γ_{1k} , were used as individual sequenceness indicators in the correlations in Fig. 4F,G. The
494 state- and subject-specific random effects are indicated by ζ . Correlations between random
495 effects were estimated. Model comparisons were conducted using likelihood-ratio tests by
496 comparing models that included the noise transitions $T(\epsilon)$ with versus without the fixed
497 effect regressor of distance (sequenceness), or without the condition interaction terms to the
498 full models that included these terms. The random effects structure was kept constant across
499 these comparisons.

500 T-tests pertaining to sequenceness results (number of steps, etc.) are one-tailed, given
501 our *a priori* expectation of larger sequenceness in the hippocampus compared to the various
502 controls.

503 Alternative Task Transition Matrices

504 As mentioned in the main text, for reasons of model comparability we used the 1-step
505 transitions of the task as a basis to test alternative replay models. The 1-step transition
506 matrix simply reflects from which state one could proceed to which other states in one trial.
507 The alternative task transition matrices were based on the assumption that the hippocampus
508 has access to only partial state information, and hence correspond to transition matrices
509 defined over subsets of states.

For instance, to compute the transition matrix of the “stimulus model” we defined \mathcal{S}_{Fy}^{stim}
as the subset of states in which Fy was the stimulus:

$$\mathcal{S}_{Fy}^{stim} = \{(Fy)Fy, (Fo)Fy, (Hy)Fy, (Ho)Fy\}.$$

510 \mathcal{S}_{Fo}^{stim} , \mathcal{S}_{Hy}^{stim} , \mathcal{S}_{Ho}^{stim} were the corresponding subsets of states in which Fo, Hy and Ho were
511 the stimuli, respectively. The 1-step distance matrix was then computed such that every
512 transition between two states s_i and s_j in the complete task state diagram was converted
513 into four transitions from s_i to all four states that are part of the same subset as s_j , that is
514 \mathcal{S}_j^{stim} . All resulting transitions are summed, and normalized so that all exiting transitions
515 from a state would sum to 1. The new transition between \mathcal{S}_{Fy}^{stim} and \mathcal{S}_{Fo}^{stim} would therefore
516 count within it $(Fy)Fy \rightarrow (Fy)Fo$, $(Ho)Fy \rightarrow (Fy)Fo$ and $(Hy)Fy \rightarrow (Fy)Fo$, whereas
517 the new transition between \mathcal{S}_{Fy}^{stim} and \mathcal{S}_{Ho}^{stim} would only count within it $(Fo)Fy \rightarrow (Fy)Ho$.
518 After normalization, these would be 3/8 and 1/8, respectively.

519 For the other alternative models, we defined subsets of states that have the same current
520 attended category, and subsets of states that have the same current and previous attended
521 categories, and then computed the transition matrices as described above. The 1-step

522 transition matrices of these alternative models are shown in Figure 5A-C. The reverse replay
523 transition matrix was simply the transpose of the full task 1-step transition matrix.

524 Synthetic fMRI Data and Noise Simulations

525 In order to estimate to what extent training the classifiers on sequential data influenced
526 the sequenceness of their predictions, we simulated, for each participant, individually spatio-
527 temporally matched fMRI noise, and applied the classifiers to these data. For each partici-
528 pant and resting state session, we first extracted fMRI data from the hippocampus and the
529 orbitofrontal cortex. As in the classification analyses, we applied linear detrending to each
530 voxel. We then estimated the average standard deviation of the voxels within these regions, as
531 well as the average autocorrelation using an AR(1) model in R. Next, we used the neuRosim
532 toolbox in R⁵¹ to simulate fMRI noise with the same standard deviation and temporal
533 autocorrelation as the real data. Finally, we used AFNI's 3dFWHMx and 3dBlurToFWHM
534 functions to first estimate the spatial smoothness of the real data, and then smooth the
535 simulated noise until it has the same effective smoothness. For each existing resting-state
536 run, matched noise data with the same number of TRs and voxels were generated. Figure
537 S1 (SI) shows the temporal and spatial smoothness of the real and simulated data separately
538 for each run. In all cases, the properties of the simulated data did not differ from the real
539 data, paired t-tests, all $ps > .05$.

540 Finally, we applied each participant's classifier to the matched noise data. The classifier
541 was identical to the classifier that was used in estimating the sequences of states from
542 the real data. The resulting sequence of predicted states reflects the bias of the classifier
543 to make sequential predictions because of pattern overlap in the training set, even when
544 applied to noise, as well as any tendency of the classifier to decode certain states more
545 often than others. We therefore used the sequence of states from this analysis to construct
546 the nuisance covariate for the mixed effects models, i.e. the noise 'transition matrix,' $T(\epsilon)$,
547 and to perform the appropriate comparisons in the correlation analysis. These comparisons
548 between sequenceness in real data versus simulated noise in the correlation and mixed effect
549 analyses indicated that the noise sequenceness $T(\epsilon)$ indeed explained a significant amount
550 of sequential variability of the decoded states (see Figs. 3F,G, 4B, D), and thus served as a
551 powerful control. Together with the permutation tests (Fig. 3B-D, 3F,G), the comparisons
552 across brain regions (Fig. 4E) and the within-participant comparisons between the PRE,
553 INSTR and TASK conditions (3B-D, H and 4A-D), our approach represents a stringent
554 control of potential biases.

555 **Data Availability**

556 All raw fMRI data, and the sequence of decoded states used to generate results in Figures
557 2-5 will be made publicly available upon publication.

558 **Code Availability**

559 All code used to generate results in Figures 2-5 will be made publicly available upon publi-
560 cation.

561 **Author Contributions**

562 NWS, and YN designed research. NWS conducted research. NWS and YN analyzed and
563 interpreted the data and wrote the manuscript.

564 **Acknowledgments**

565 This research was funded by NIH grant R01DA042065 and funding from John Templeton
566 Foundation. The opinions expressed in this publication are those of the authors and do not
567 necessarily reflect the views of the John Templeton Foundation or those of NIH. We thank
568 Nathaniel Daw, Christian Doeller, Eran Eldar and David Tank for helpful comments on this
569 research and/or previous versions of the manuscript.

570 **References**

- 571 1. Scoville, W. & Milner, B. Loss of recent memory after bilateral hippocampal lesions.
572 Journal of Neurology, Neurosurgery & Psychiatry **20**, 11–21 (1957).
- 573 2. Squire, L. R. Memory and the Hippocampus : A Synthesis From Findings With Rats,
574 Monkeys, and Humans. Psychological Review **99**, 195–231 (1992).
- 575 3. Eichenbaum, H, Dudchenko, P, Wood, E, Shapiro, M & Tanila, H. The hippocampus,
576 memory, and place cells: is it spatial memory or a memory space? Neuron **23**, 209–26 (1999).
- 577 4. O'Keefe, J. & Nadel, L. The hippocampus as a cognitive map (Oxford University Press,
578 Oxford, 1978).
- 579 5. McKenzie, S. et al. Hippocampal representation of related and opposing memories develop
580 within distinct, hierarchically organized neural schemas. Neuron **83**, 202–215 (2014).

- 581 6. Constantinescu, A. O., O'Reilly, J. X. & Behrens, T. E. J. Organizing conceptual knowledge
582 in humans with a gridlike code. Science **352**, 1464–1468 (2016).
- 583 7. Tavares, R. M. et al. A Map for Social Navigation in the Human Brain. Neuron **87**, 231–243
584 (2015).
- 585 8. Aronov, D., Nevers, R. & Tank, D. W. Mapping of a non-spatial dimension by the
586 hippocampal-entorhinal circuit. Nature **543**, 719–722 (2017).
- 587 9. Foster, D. J. & Knierim, J. J. Sequence learning and the role of the hippocampus in rodent
588 navigation. Current Opinion in Neurobiology **22**, 294–300 (2012).
- 589 10. Wikenheiser, A. M. & Redish, A. D. Decoding the cognitive map: Ensemble hippocampal
590 sequences and decision making. Current Opinion in Neurobiology **32**, 8–15 (2014).
- 591 11. Skaggs, W. E. & McNaughton, B. L. Replay of neuronal firing sequences in rat hippocampus
592 during sleep following spatial experience. Science **271**, 1870–1873 (1996).
- 593 12. Johnson, A. & Redish, D. Neural ensembles in CA3 transiently encode paths forward of the
594 animal at a decision point. Journal of Neuroscience **27**, 12176–89 (2007).
- 595 13. Karlsson, M. P. & Frank, L. M. Awake replay of remote experiences in the hippocampus.
596 Nature Neuroscience **12**, 913–918 (2009).
- 597 14. Carr, M. F., Jadhav, S. P. & Frank, L. M. Hippocampal replay in the awake state: a potential
598 substrate for memory consolidation and retrieval. Nature Neuroscience **14**, 147–53 (2011).
- 599 15. Girardeau, G., Benchenane, K., Wiener, S. I., Buzsáki, G. & Zugaro, M. B. Selective
600 suppression of hippocampal ripples impairs spatial memory. Nature Neuroscience **12**,
601 1222–1223 (2009).
- 602 16. Schuck, N. W., Cai, M. B., Wilson, R. C. & Niv, Y. Human Orbitofrontal Cortex Represents
603 a Cognitive Map of State Space. Neuron **91**, 1402–1412 (2016).
- 604 17. Tong, S. & Chang, E. Support vector machine active learning for image retrieval in
605 Proceedings of the ninth ACM international conference on Multimedia **October** (ACM
606 Press, New York, New York, USA, 2001), 107–118. doi:10.1145/500156.500159.
- 607 18. Peigneux, P. et al. Are Spatial Memories Strengthened in the Human Hippocampus during
608 Slow Wave Sleep ? Neuron **44**, 535–545 (2004).
- 609 19. Deuker, L. et al. Memory Consolidation by Replay of Stimulus-Specific Neural Activity.
610 Journal of Neuroscience **33**, 19373–19383 (2013).

- 611 20. Staresina, B. P., Alink, A., Kriegeskorte, N. & Henson, R. N. Awake reactivation predicts
612 memory in humans.
613 Proceedings of the National Academy of Sciences of the United States of America **110**,
614 21159–64 (2013).
- 615 21. Axmacher, N., Elger, C. E. & Fell, J. Ripples in the medial temporal lobe are relevant for
616 human memory consolidation. Brain **131**, 1806–1817 (2008).
- 617 22. Wilson, R. C., Takahashi, Y. K., Schoenbaum, G. & Niv, Y. Orbitofrontal cortex as a
618 cognitive map of task space. Neuron **81**, 267–79 (2014).
- 619 23. Sutton, R. S.
620 Integrated architectures for learning, planning, and reacting based on approx dynamic prog
621 in Proceedings of the 7th International Conference on Machine Learning (1990), 216–224.
622 doi:10.1.1.51.7362.
- 623 24. Van Seijen, H. & Sutton, R. S. A Deeper Look at Planning as Learning from Replay.
624 Proceedings of the 32nd International Conference on Machine Learning **37** (2015).
- 625 25. Russek, E. M., Momennejad, I., Botvinick, M. M. & Gershman, S. J. Predictive
626 representations can link model-based reinforcement learning to model-free mechanisms.
627 bioRxiv **083857**. doi:10.1101/083857 (2016).
- 628 26. Kaplan, R., Schuck, N. W. & Doeller, C. F. The Role of Mental Maps in Decision-Making.
629 Trends in Neurosciences **40**, 256–259 (2017).
- 630 27. Bergmann, T. O., Mölle, M., Diedrichs, J., Born, J. & Siebner, H. R. Sleep spindle-related
631 reactivation of category-specific cortical regions after learning face-scene associations.
632 NeuroImage **59**, 2733–2742 (2012).
- 633 28. Kurth-Nelson, Z., Economides, M., Dolan, R. J. & Dayan, P. Fast sequences of non-spatial
634 state representations in humans. Neuron **91**, 194–204 (2016).
- 635 29. Cox, R., Hofman, W. F., de Boer, M. & Talamini, L. M. Local sleep spindle modulations in
636 relation to specific memory cues. NeuroImage **99**, 103–110 (2014).
- 637 30. Rasch, B., Buchel, C., Gais, S. & Born, J. Odor Cues During Slow-Wave Sleep Prompt
638 Declarative Memory Consolidation. Science **315**, 1426–1429 (2007).
- 639 31. Antony, J. W., Gobel, E. W., O’Hare, J. K., Reber, P. J. & Paller, K. A. Cued memory
640 reactivation during sleep influences skill learning. Nature Neuroscience **15**, 1114–1116 (2012).
- 641 32. Siapas, A. G. & Wilson, M. A. Coordinated interactions between hippocampal ripples and
642 cortical spindles during slow-wave sleep. Neuron **21**, 1123–1128 (1998).

- 643 33. Ji, D. & Wilson, M. A. Coordinated memory replay in the visual cortex and hippocampus
644 during sleep. Nature Neuroscience **10**, 100–107 (2007).
- 645 34. Lee, A. K. & Wilson, M. A. Memory of Sequential Experience in the Hippocampus during
646 Slow Wave Sleep. Neuron **36**, 1183–1194 (2002).
- 647 35. Schiller, D. et al. Memory and Space: Towards an Understanding of the Cognitive Map.
648 Journal of Neuroscience **35**, 13904–13911 (2015).
- 649 36. Tolman, E. C. Cognitive maps in rats and men. Psychological Review **55**, 189–208 (1948).
- 650 37. Fortin, N. J., Agster, K. L. & Eichenbaum, H. B. Critical role of the hippocampus in
651 memory for sequences of events. Nature Neuroscience **5**, 458–62 (2002).
- 652 38. Schapiro, A. C., Kustner, L. V. & Turk-Browne, N. B. Shaping of object representations in
653 the human medial temporal lobe based on temporal regularities. Current Biology **22**,
654 1622–1627 (2012).
- 655 39. Stachenfeld, K. L., Botvinick, M. M. & Gershman, S. J. The hippocampus as a predictive
656 map. Nature Neuroscience **20**, 1643–1653 (2017).
- 657 40. Bradfield, L. A., Dezfouli, A., van Holstein, M., Chieng, B. & Balleine, B. W. Medial
658 Orbitofrontal Cortex Mediates Outcome Retrieval in Partially Observable Task Situations.
659 Neuron, 1–13 (2015).
- 660 41. Howard, J. D. & Kahnt, T. Identity-specific reward representations in orbitofrontal cortex
661 are modulated by selective devaluation. Journal of Neuroscience **37**, 3473–16 (2017).
- 662 42. Nogueira, R. et al. Lateral orbitofrontal cortex anticipates choices and integrates prior with
663 current information. Nature Communications **8**, 14823 (2017).
- 664 43. Schuck, N. W. et al. Medial Prefrontal Cortex Predicts Internally Driven Strategy Shifts.
665 Neuron **86**, 331–340 (2015).
- 666 44. Doeller, C. F., Barry, C. & Burgess, N. Evidence for grid cells in a human memory network.
667 Nature **463**, 657–61 (2010).
- 668 45. Jacobs, J et al. Direct recordings of grid-like neuronal activity in human spatial navigation.
669 Nature Neuroscience **16**, 1188–1190 (2013).
- 670 46. Ebner, N. C., Riediger, M. & Lindenberger, U. FACES - A database of facial expressions in
671 young, middle-aged, and older women and men: Development and validation.
672 Behavior Research Methods **42**, 351–362 (2010).
- 673 47. Bates, D., Mächler, M., Bolker, B. & Walker, S. Fitting Linear Mixed-Effects Models Using
674 lme4. Journal of Statistical Software **67**, 51 (2015).

- 675 48. R Core Team. R: A Language and Environment for Statistical Computing Vienna, Austria,
676 2015.
- 677 49. Deichmann, R, Gottfried, J., Hutton, C & Turner, R. Optimized EPI for fMRI studies of the
678 orbitofrontal cortex. NeuroImage **19**, 430–441 (2003).
- 679 50. Chang, C.-c. & Lin, C.-j. LIBSVM 2011. doi:10.1145/1961189.1961199.
- 680 51. Welvaert, M., Durnez, J., Moerkerke, B., Verdoolaege, G. & Rosseel, Y. neuRosim : An R
681 Package for Generating fMRI Data. Journal of Statistical Software **44**, 1–18 (2011).